POLARIZATION MEASUREMENTS OF ASTEROIDS AT 25 μm WITH ISOPHOT *

T.G. Müller[1], J.S.V. Lagerros[2,3], U. Klaas[4], and A. Erikson[5]
[1]ISO Data Centre, ESA Astrophysics Division, Villafranca del Castillo, Spain;
[2]Five College Radio Astronomy Observatory, Massachusetts, USA;
[3]Astronomiska observatoriet, Uppsala, Sweden;
[4]Max-Planck-Institut für Astronomie, Heidelberg, Germany;
[5]DLR, Berlin, Germany

ABSTRACT

The asteroids (6) Hebe and (9) Metis were observed at $\lambda = 25\,\mu$m with ISOPHOT onboard the Infrared Space Observatory (ISO). The on- and off-source measurements have been analysed with a special data reduction method to achieve reliable photometric and polarimetric results. In parallel a previously established thermophysical model has been extended to cover also polarimetric aspects.
The model absolute fluxes are in good agreement with the photometric results. Although no linear polarization was detected, the upper limits together with the extended model enable us to put useful constraints on the regolith properties of the target asteroids. The derived detection limits are compared to model polarization, by spanning a range in surface roughness, refractive index, and thermal inertia parameter space. The Metis observations favor a low refractive index and high surface roughness, but the Hebe observations are inconclusive since they coincided with a minimum in the polarization curve.

Key words: ISO; Infrared Astronomy; Asteroids; Polarimetry; Regoliths; Asteroid Surfaces.

1. INTRODUCTION

With improving observation techniques, the study of the thermal emission from asteroids has the potential of becoming a very important tool in investigating their fundamental physical properties. One such possibility is to study the state of polarization. The disk integrated thermal emission has been observed to be linearly polarized at a degree of 0.2–0.6 % for (1) Ceres at 10 μm (Johnson *et al.* 1983) and 1.6 % for Io at 4.76 μm (Goguen and Sinton 1985). This can be explained by the scattering of sub-surface emission in the regolith into the empty space, which results in polarization according to Fresnel's equations. The electrical vector becomes parallel to the scattering plane, that is the plane containing the surface normal and the direction of propagation. This is seen in the disk resolved microwave emission from the Moon (Heiles and Drake 1963; Clegg and Carter 1970) and Mercury (Mitchell and De Pater 1994).
The asteroids are in general too small and too distant to be disk resolved, thus in case of symmetry no polarization is expected. A number of effects are, however, causing asymmetries in the emission. For an elongated shape there is a preferred orientation of the surface normals, and consequently of the electrical vectors, causing the disk integrated flux to be polarized. Lagerros (1997) demonstrated how the degree of polarization should increase with more elongated shape, and smoother surface. Johnson *et al.* (1983) explained the observed polarization by asymmetries in the temperature distribution across the disk due to the thermal inertia and the solar phase angle.
Now with ISOPHOT (Lemke *et al.* 1996), the imaging photopolarimeter on board the Infrared Space Observatory ISO (Kessler *et al.* 1996), it has become feasible to perform sensitive polarization measurements down to flux densities of 1–2 Jy. Here we report the results of the ISOPHOT polarization measurements of the asteroids (6) Hebe and (9) Metis, focusing on the data reduction method. The data are interpreted by extending a thermophysical model developed and calibrated throughout a series of papers (Lagerros 1996a, 1996b, 1997, 1998; Müller and Lagerros 1998). The theoretical background of the model extension and a detailed interpretation of the results can be found in Lagerros *et al.* (1999).
The observations and the data reduction are presented in Section 2., the target asteroids and the model improvements in Section 3. The non-detection of any polarization puts constraints on the physical properties of the surface material, as discussed in Section 4. and summarized in Section 5.

2. OBSERVATIONS

The asteroids (6) Hebe and (9) Metis were selected based on their excellent visibility during the last

*ISO is an ESA project with instruments funded by ESA Member States (especially the PI countries: France, Germany, the Netherlands and the United Kingdom) and with the participation of ISAS and NASA.

Table 1. Epochs and pointings of the (6) Hebe and (9) Metis observations, including the background measurements. The ISO pointing information is taken from ISO IIPH data products, the ISOcentric asteroid positions are calculated from Chebycheff coefficients provided by Bureau des Longitudes, Paris

UT Start of Obs.	ISO Pointing RA Dec	Asteroid Position (J2000.0) RA Dec (ISO-centric)	RA Dec (geocentric)	Pointing Offset
(6) Hebe 1998-Apr-02				
07:02:54	$17^{h}23^{m}45^{s}90$ $-05°13'57''0$	$17^{h}24^{m}07^{s}61$ $-05°09'57''3$	$17^{h}24^{m}09^{s}71$ $-05°09'57''0$	$6'43''3$
07:43:01	$17^{h}24^{m}08^{s}01$ $-05°09'48''6$	$17^{h}24^{m}08^{s}01$ $-05°09'48''5$	$17^{h}24^{m}10^{s}32$ $-05°09'48''5$	$0''1$
(9) Metis 1998-Mar-29				
19:52:31	$04^{h}49^{m}55^{s}60$ $+25°04'47''0$	$04^{h}50^{m}16^{s}61$ $+25°04'37''6$	$04^{h}50^{m}14^{s}00$ $+25°04'28''6$	$4'45''8$
20:32:37	$04^{h}50^{m}19^{s}73$ $+25°04'44''6$	$04^{h}50^{m}19^{s}74$ $+25°04'44''6$	$04^{h}50^{m}17^{s}29$ $+25°04'35''4$	$0''1$

months of the ISO mission. Furthermore, based on lightcurve studies and occultation measurements, there is fairly good information available on their shapes, spin-vectors and sizes. Modelling the thermal flux and shape-asymmetry at the expected observing time gave sufficiently high source-to-background contrast to test our hypothesis of disk integrated polarized thermal emission.

2.1. ISOPHOT observations

ISOPHOT is equipped with two sets of polarizers to be used in the mid-IR at 25 μm or far-IR at 170 μm. Because of the brightness limitations we used only the three 25 μm-polarizers with orientation angles of 0°, 120°, and 240° w.r.t. the spacecraft y-axis (Wolf *et al.* 1994). Each of them consists of a silicon substrate with an incarved grating, spaced with 0.4 μm. The bandpass is comparable to the IRAS 25 μm bandpass. The central wavelength is $\lambda_c = 23.81\,\mu$m, the width $\lambda_\Delta = 9.18\,\mu$m, and the average relative system response $R_{\rm mean} = 0.39$ (Klaas *et al.* 1994). Table 1 summarizes the observation epochs and the asteroid and background positions. Aspect data are given for the asteroids in Table 2. The integration time per polarizer was 128 s to allow for signal stabilisation with the P2-detector, using the default 79″ circular aperture (ISOPHOT observing mode P50). Within this observing mode, 4 full polarizer cycles plus one additional 0°-polarizer position, a staring observation without polarizer and an internal reference measurement for photometric calibration have been obtained, both on- and off-source (Figure 1). The off-source observations were obtained before the on-source ones with 5′ and 7′ angular separation from the asteroid (see Table 1). The on-source signal was obtained in "Solar System Tracking Mode". The pointing uncertainty of ISO, which is in the order of a few arcseconds, is not influencing the results, since the aperture size is 79″. The signals of the Metis on-source observational sequence, before and after correcting for a long-term drift, are shown in Figure 2 and Figure 3, respectively. With 128 s integration time per polarizer position we minimized the total noise contribution. Although a longer integration time would lower the *photon-* and *detector-noise*, the $1/f$-*noise* and the signal drift influence would make the total S/N worse. With this optimized integration time we reached a S/N of 210 for Metis and 145 for Hebe (after drift correction). Performing 4 full cycles on both asteroids as well as on the backgrounds exceeded the typical duration of polarization measurements with ISO where usually only 2 cycles were done.

Table 2. Aspect data: heliocentric distance r, geocentric distance Δ, solar phase angle $\alpha_{\rm ph}$, ecliptic longitude λ and latitude β.

UT Date	r [km]	Δ [km]	α [°]	λ [°]	β [°]
(6) Hebe 1998-Apr-02					
07:43:01	2.7380	2.2205	20.0	260.6	18.0
(9) Metis 1998-Mar-29					
20:32:37	2.1187	2.3323	25.3	74.2	2.6

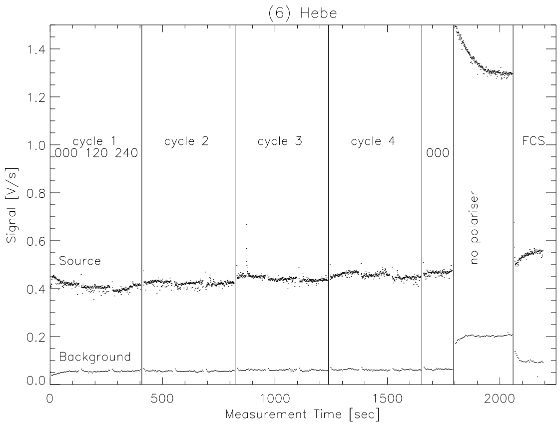

Figure 1. The full measurement sequence for (6) Hebe. Each sequence contains 4 cycles with all 3 polarizers, a repetition of the 0°-polarizer, a staring observation without polarizer and an internal calibrator measurement. The measured signal [V/s] are corrected for a long-term drift of the signal.

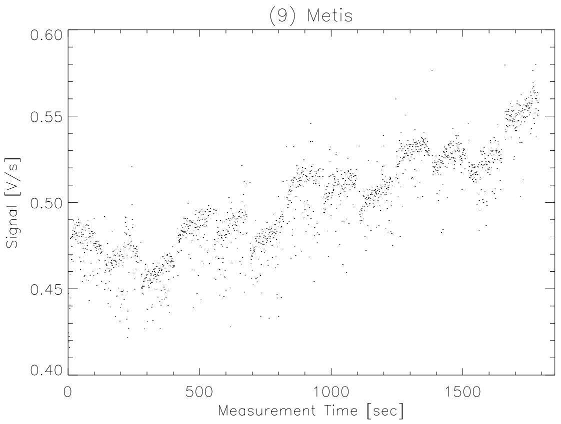

Figure 2. The enlarged, but still uncorrected, on-source measurement sequence for (9) Metis. The long-term drift of the measured signal is visible.

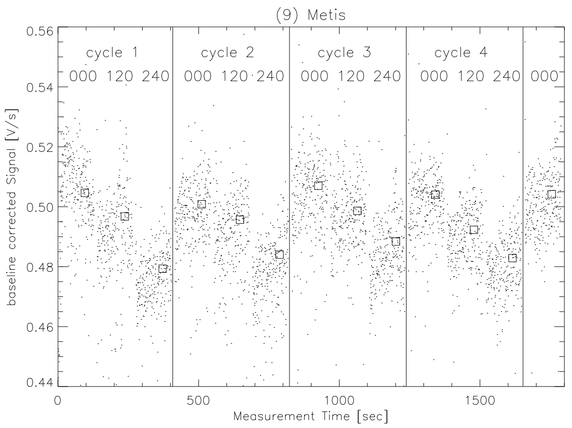

Figure 3. The enlarged on-source measurement sequence for (9) Metis. The measured signal [V/s] are corrected for a long-term drift. The derived signal values are indicated with boxes.

2.2. Data reduction

ISOPHOT Interactive Analysis (PIA)[1] V7.1 was used for the standard data reduction up to signal level, including linear ramp fitting, deglitching on ramp and signal level, reset interval correction and orbit dependent dark signal subtraction (Gabriel *et al.* 1997). The general detector drift has been corrected for by dividing by a second order fit to the last 3 polarizer cycles, excluding the first one when the signal was not yet stabilised. The signal per polarizer (see Table 3) has been determined by averaging the second half of the measured signals in each polarizer.
For the polarization analysis we used a specially designed FORTRAN code which read in the derived signal values and produced all relevant output data as described in Klaas *et al.* (1999). The determination of Stokes parameters and polarization values are based on the formula for imperfect polarizers as given in Serkowski (1962). A polarizer efficiency of $P' = (90 \pm 3)\,\%$ was measured during ground calibration. Sky background subtraction was performed by subtracting the Stokes parameters “off-target” from the ones “on-target”.

[1]PIA is a joint development by the ESA Astrophysics Division and the ISOPHOT consortium.

2.3. Instrumental polarization and uncertainty calculation

The instrumental polarization for the P2, 25 μm-configuration has been determined from measurements of unpolarized sources, stars (α Tau, α Boo and γ Dra) and background fields, using the same observational set-up. The measurements show a highly reproducible pattern yielding $P_{\rm inst} = (2.96 \pm 0.20)\,\%$, in the direction $\theta_{\rm inst} = -18°63 \pm 1°45$, counted w.r.t. the ISO spacecraft y-axis. This observed instrumental polarization is taken into account according to the procedure described in Klaas *et al.* (1999).
Here we quote Gaussian uncertainties (partial derivatives are summed up quadratically). From Figure 1 to Figure 3 one can see that the reproducibility of the signals in the different polarizer settings is a representative measure for the signal uncertainty. The 3 %-error of the polarizer efficiency is also taken into account. The dominant factor in the determination of the total uncertainty is the source-to-background contrast. For Metis the ratio was approximately 2, for Hebe larger than 6, leading to 1 σ-uncertainties for the polarization degree of less than 1 %.

3. THERMOPHYSICAL MODELING OF THE ASTEROIDS

The model derives the disk integrated Stokes parameters for the thermal IR emission by calculating

$$\mathbf{S}_{\rm disk} = \frac{\mathbf{1}}{\pi \mathbf{\Delta^2}} \oint_{\mathbf{A}} \mathbf{\Lambda B}_\lambda(\mathbf{T}) \mu \, \mathbf{dA}, \qquad (1)$$

in which Δ is the distance to the observer, T the surface temperature, $B_\lambda(T)$ the corresponding black body emissive power, $\mathbf{\Lambda}$ an emissivity and surface roughness correction discussed below, and μ the direction cosine projecting the surface element dA towards the observer. In brief the major steps in the model calculations are:

1. Define a shape. The model is capable of using anything from a sphere to a highly irregular object. The asteroids are in this case described by ellipsoids. The dimensions have been determined from ground based observations.

2. Compute the position and the orientation of the asteroid relative to the Sun and the observer.

3. Approximate the surface by a set of triangular facets.

4. Compute the illumination and viewing geometry relative to the local horizon of each facet.

5. Derive the facet temperature taking into account the absorbed solar radiation, the thermal emission and the conduction of heat into the surface material. When the asteroid is rotating, the heat conduction results in a lag of the peak temperature, night side emission and lower day side emission.

6. Apply a emissivity and surface roughness correction to the brightness temperature, in order to obtain the Stokes parameters of each facet. The small scale roughness randomizes the scattering planes of the surface. As a result the emission becomes depolarized and enhanced or "beamed" towards the solar direction. The roughness is described by hemispherical craters covering a smooth surface, and the emissivity is computed from the optical constants assumed for the surface material at the observed wavelength.

7. Obtain the disk integrated flux by adding the contributions from each facet.

The surface inside the crater is considered to be smooth such that the light scattering properties of the material are described by Snell's law and the Fresnel's equations. These laws are given e.g. by Modest (1993) in the case the imaginary part of the refractive index cannot be neglected. The subsurface emission is partially reflected inwards, as described by the Fresnel coefficients $R_\perp$ and $R_\|$ for the beams perpendicular to and parallel, to the scattering plane, respectively. The coefficients of interest in the 4×4 scattering matrix are

$$F_{11} = \frac{1}{2n^2}(2 - R_\perp - R_\|), \quad F_{21} = \frac{1}{2n^2}(R_\perp - R_\|),$$
$$F_{31} = 0, \quad F_{41} = 0 \tag{2}$$

4. RESULTS AND DISCUSSION

4.1. Polarization

Table 3 lists the polarization results per polarizer cycle. The polarizer positions are characterised by "000, 120, 240", the first cycle (see Figure 2) has been ignored, since the signal was not yet stabilised. The orientation and degree of polarization can be obtained from each cycle. Underneath the results of the individual cycles, Table 3 contains the averaged results (summation of vectors). Both asteroid measurements result in approximately 0.5 % polarization. In the case of small polarization degrees one uses the so-called debiased polarization degree $P_{\rm debias} = \sqrt{P^2 - dP^2}$, according to the method described by Wardle and Kronberg (1974). This yields "zero"-polarization for both asteroids.

4.2. Photometry

The last part of each observation contained a normal photometric measurement ('open polarizer') together with a measurement of the internal reference source

Table 3. Polarization results for (6) Hebe and (9) Metis. The signals are corrected for a long-term detector drift. The effects of instrumental polarization are already accounted for in the derived degree of linear polarization $\pi_{\rm L}$ and orientation angle ψ. The means over the three cycles 2, 3, and 4 (summation of vectors) are also given.

Cyc. Pos.	Signals [mV/s] Src.	Bg.	Polarization $\pi_{\rm L}$ [%]	ψ [°]
(6) Hebe				
000	426.18	57.64		
120	413.87	55.23	0.61 ± 0.77	$+25.91 \pm 36.87$
240	406.07	55.03		
000	424.62	58.84		
120	410.20	57.76	1.19 ± 0.81	$+14.55 \pm 18.63$
240	400.94	55.42		
000	426.96	58.09		
120	419.77	55.97	0.82 ± 0.75	-39.73 ± 28.22
240	405.49	56.75		
Mean				
000	425.92	58.19		
120	414.61	56.32	0.53 ± 0.81	$+4.53 \pm 41.02$
240	404.17	55.73		
(9) Metis				
000	505.09	171.79		
120	497.57	167.20	0.60 ± 0.77	-80.57 ± 33.89
240	484.76	164.88		
000	507.61	170.35		
120	498.96	168.15	0.34 ± 0.70	$+54.35 \pm 64.61$
240	488.97	165.99		
000	503.83	171.21		
120	492.58	168.15	1.13 ± 0.71	$+49.24 \pm 19.69$
240	483.88	162.97		
Mean				
000	505.51	171.12		
120	496.37	167.83	0.50 ± 0.72	$+62.07 \pm 43.05$
240	485.87	164.61		

(FCS). The signal ratios *source/FCS* have been determined by averaging the last stable part of the measurement. The photometric calibration was done by using the actual response of the detector, corrected by a few percent for non-linearity (Huth and Schulz, priv. comm.). A color correction of 1.10, corresponding to a black body spectrum of 250 K, was applied to obtain monochromatic fluxes at 25 μm (Laureijs et al. 1998). The photometric uncertainties for sources with flux densities between 10 and 200 Jy, measured with the ISOPHOT P2-detector, are less than 15 % (Klaas *et al.* 1998). The results are summarised in Table 4. In the case of Metis the background was a factor of 2 higher than measured by COBE/DIRBE. The reason is unclear, but could be due to a surface brightness gradient in the $0\overset{\circ}{.}7 \times 0\overset{\circ}{.}7$ COBE-beam compared to the $79''$ ISOPHOT aperture.

4.3. Comparisons with model calculations

Model thermal emission and polarization curves were produced for a wide range of parameters. A few of these curves are shown in Figures 4 and 5, in order to illustrate the influence of roughness and dielectric properties on the flux and polarization. In general,

Table 4. *Photometry results for (6) Hebe and (9) Metis.*

UT		$\lambda\,[\mu\mathrm{m}]$	F_ν [Jy]	σ_{F_ν} [Jy]
(6) Hebe				
1998-Apr-02	08:17:00	25.0	36.9	5.5
(9) Metis				
1998-Mar-29	21:06:00	25.0	37.9	5.7

increasing the surface roughness lowers the degree of linear polarization and enhances the thermal emission in the solar direction. A higher refractive index increases the degree of polarization, and decreases the absolute flux by lowering the emissivity.
Considering the observational uncertainties, the uncertainties in the quoted diameters, and the uncertainties in the assumed thermophysical parameters, the observed and predicted absolute fluxes are in good agreement for both objects.
Since no polarization was detected, the derived electric vectors are randomly oriented. The predicted orientation angle ψ relative to the projected spin vector is shown for (9) Metis in Figure 5. Although ψ varies substantially for both asteroids during the rotational period, during one polarizer cycle of 3×128 *sec* is does not change significantly. The time averaged Stokes parameters have an orientation close to $\psi = 0$.

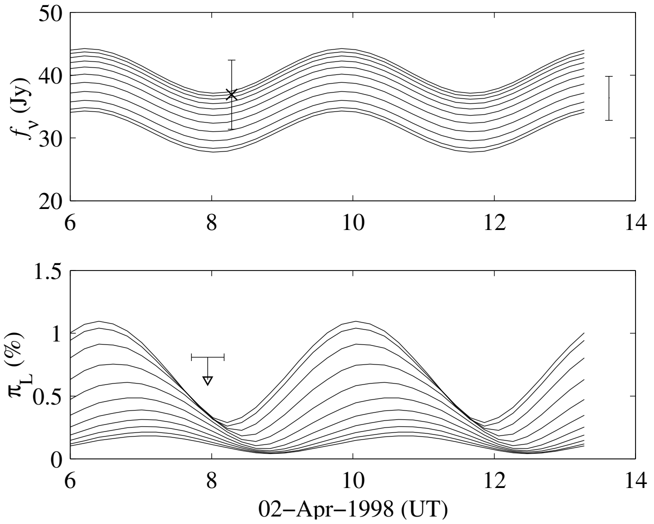

Figure 4. Model thermal lightcurves for (6) Hebe at $25\,\mu$m*, assuming a refractive index of* $m = 2$*, and r.m.s slopes* $\rho = 0,\ 0.1,\ \ldots,\ 1.0$. **Upper panel**: *Observed and predicted flux* f_ν*. The model fluxes increase with the surface roughness* ρ*. To the right is the typical error bar for the model fluxes, due to the uncertainty in the occultation diameter only.* **Lower panel**: *The time span and detection limit of linear polarization* π_L*. The predicted degree of linear polarization increases with lower surface roughness. The upper limit by the ISOPHOT observation is indicated.*

The derived 1σ-levels in Table 3 were taken as de-

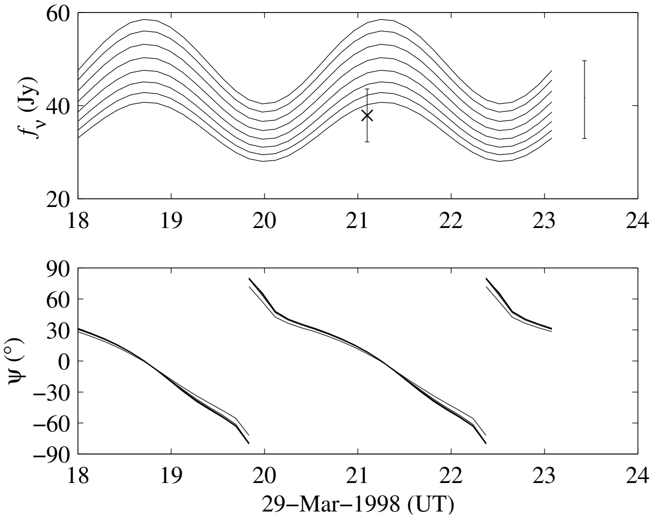

Figure 5. Model thermal lightcurves for (9) Metis at $25\,\mu$m*, assuming a r.m.s slope* $\rho = 0.7$ *and refractive indexes of* $m = 1.2,\ 1.6,\ \ldots,\ 4.0$. **Upper panel**: *Observed and predicted flux* f_ν*. The model fluxes increase with lower refractive index n. To the right is the typical error bar for the model fluxes, due to the uncertainty in the occultation diameter only.* **Lower panel**: *The orientation angle* ψ *of the modeled polarization, relative to the projected spin vector.*

tection limits of polarization. Comparison of these upper limits with the predicted degrees of linear polarization, puts constraints on the parameter space (see also Lagerros *et al.* 1999). The (6) Hebe observations unfortunately took place during a minimum in the polarization lightcurve (Figure 4). Thus, it is not possible to put tight constraints on the parameter space using the Hebe data.

5. CONCLUSION

The ISOPHOT measurements presented here were the first attempts to detect polarized thermal emission from asteroids. Although we did not find any significant polarization, despite good sensitivity, these observations add valuable constraints to our knowledge of the regoliths of asteroids. The upper polarization limit for the Metis observations narrows down the range for surface roughness and refractive index. A high refractive index is unlikely because of composition and porosity expected for the surface material. A more detailed discussion can be found in Lagerros *et al.* (1999).

Acknowledgements

Part of this work was supported by The Swedish Foundation for International Cooperation in Research and Higher Education (STINT). The work of W. Krätschmer (Max-Planck-Institut für Kernphysik, Heidelberg) in purchasing and characterizing ISOPHOT's MIR polarizers is acknowledged.

REFERENCES

Clegg, P.E. and Carter, B.S. 1970, MNRAS **148**, 261

Gabriel, C., Schulz, B., Acosta–Pulido, J. A. *et al.* 1997, Proc. of ADASS VI, 112

Goguen, J.D. and Sinton, W.M. 1985, Science **230**, 65

Heiles, C.E. and Drake, F.D. 1963, ICARUS **2**, 281

Johnson, P.E., Kemp, J.C., Lebofsky, M.J. and Rieke, G.H. 1983, ICARUS **56**, 381

Kessler M.F., Steinz J.A., Anderegg M.E., *et al.* 1996 A&A 315, L27

Klaas, U., Krüger, H.Heinrichsen, I. *et al.* 1994, ISOPHOT Observer's Manual, ESA/ESTEC, Noordwijk, Version 3.1

Klaas, U., Laureijs, R.J., Radovich, M. and Schulz, B. 1998, Calibration Accuracies (http://www.iso.vilspa.esa.es/manuals/PHT/accuracies/pht_accuracies20/)

Klaas, U., Laureijs, R.J. and Clavel, J. 1999, ApJ **512**, 157

Lagerros, J.S.V. 1996a, A&A, **310**, 1 011

Lagerros, J.S.V. 1996b, A&A, **315**, 625

Lagerros, J.S.V. 1997, A&A, **325**, 1 226

Lagerros, J.S.V. 1998, A&A, **332**, 1 123

Lagerros, J.S.V., Müller, T.G., Klaas, U. and Erikson, A. 1999, ICARUS, in press

Laureijs R.J., Klaas U., Richards PlJ. *et al.* 1998, ISOPHOT Data Users Manual, SAI/95-220/Dc, Version 4.0, Appendix C: Colour Corrections

Lemke D., Klaas U., Abolins J., *et al.* 1996, A&A 315, L64

Mitchell, D.L. and De Pater, I. 1994, ICARUS **110**, 2

Modest, M.F. 1993, Radiative Heat Transfer, McGraw-Hill Publishing Company, New York

Müller, T.G., Lagerros, J.S.V. 1998, A&A, **338**, 340

Serkowsky, K. 1962, Advances in Astronomy and Astrophysics (K. Zdenek, Ed.), 290, Academic Press

Wardle, J. and Kronber, P. 1974, Astrophys. J. **194**, 249

Wolf, J. *et al.* 1994, Opt. Engineering **33**, 26